Contribution of ion-induced nucleation to new particle formation: Methodology and its application to atmospheric observations in Boulder, Colorado

Kenjiro Iida,[1] Mark Stolzenburg,[1] Peter McMurry,[1] Matthew J. Dunn,[2] James N. Smith,[2] Fred Eisele,[2] and Pat Keady[3]

Received 5 February 2006; revised 13 June 2006; accepted 26 July 2006; published 2 December 2006.

[1] This paper investigates the role of ion-induced nucleation (IIN) in new particle formation events observed near ground level at a sampling site located near Boulder, Colorado (14 March 2004 to 27 October 2005). Measurements of mobility distributions of small and intermediate ions (0.4–6.3 nm), size distributions of total particles (3 nm to 5 μm), and charged fractions (2.5–25 nm) were carried out. The relative contributions of neutral nucleation and IIN were inferred using both qualitative and quantitative analyses. First, a simple theoretical analysis is performed to show what can be learned about the initial charge state of the nucleated particles from charged fractions measured after they had grown to 3.0–5.5 nm. We found that for much of our data the charge fractions of freshly nucleated particles below 5 nm were significantly below stationary-state values, and that this tendency increased with decreasing size, indicating that neutral nucleation was dominant. However, the data also show that there were occasionally asymmetries between negative and positive charge fractions that we could not explain unless positive or negative IIN occurred to some extent. A quantitative analysis is then performed to estimate the fractional contribution of positive and negative IIN to new particle formation rates for each nucleation event observed during this period. The results show the average contribution of IIN is about 0.5% for both polarities indicating that IIN was a relatively insignificant contributor to new particle formation in this study. This result is consistent with the direct mass spectrometric measurements of sulfuric acid ion cluster compositions and concentrations performed at the same measurement site.

Citation: Iida, K., M. Stolzenburg, P. McMurry, M. J. Dunn, J. N. Smith, F. Eisele, and P. Keady (2006), Contribution of ion-induced nucleation to new particle formation: Methodology and its application to atmospheric observations in Boulder, Colorado, *J. Geophys. Res.*, *111*, D23201, doi:10.1029/2006JD007167.

1. Introduction

[2] Recent work has shown that new particles are often formed by nucleation in the atmosphere [*Kulmala et al.*, 2004]. The species and mechanisms responsible for nucleation are not well understood, and probably vary from location to location depending on the concentrations of trace species that can react to form new particles. Ion-induced nucleation (IIN) involves the condensation of vapors on positive or negative ions. Previous studies have shown that IIN is likely to be an important source of atmospheric particles in some locations [*Tammet et al.*, 1992; *Hõrrak et al.*, 1998b; *Yu and Turco*, 2000, 2001; *Lee et al.*, 2003]. Atmospheric ions are continuously formed by cosmic radiation and radioactive decay, and the ionization rate in the troposphere ranges from 2 to 30 ion pairs cm^{-3} s^{-1} [*Chalmers*, 1967; *Reiter*, 1992].

[3] The nucleation of H_2SO_4 vapor onto H_2SO_4/H_2O ion clusters is believed to be an important process and has been studied theoretically and experimentally. According to the classical theory [*Yue and Chan*, 1979], conditions that favor IIN by this process include low temperature, high relative humidity (RH), high ion production rate, and low concentrations of preexisting particles [*Laakso et al.*, 2002]. A detailed kinetic model based on experimentally obtained thermodynamic data of $H_2SO_4^-/H_2O$ ion clusters shows that IIN for this system will only occur when appropriate conditions for H_2SO_4, RH, and temperature are met [*Lovejoy et al.*, 2004]. These conditions are often met in the upper troposphere and lower stratosphere. Aircraft-based measurements [*Lee et al.*, 2003] showed that the observed time evolution of particle size distributions was consistent with predictions by the IIN model of *Lovejoy et al.* [2004]. Mass spectrometric measurements of positive ions in the upper troposphere detected the growth of positive ions up to masses as high as 2500 amu containing acetone and sulfuric

[1] Particle Technology Laboratory, University of Minnesota, Minneapolis, Minnesota, USA.
[2] Atmospheric Chemistry Division, National Center for Atmospheric Research, Boulder, Colorado, USA.
[3] Quant Technologies, LLC, Blaine, Minnesota, USA.

0148-0227/06/2006JD007167

acid [*Eichkorn et al.*, 2002]. On the other hand recent measurements of sulfuric acid ion clusters at the surface near Boulder, Colorado showed no evidence of IIN [*Eisele et al.*, 2006].

[4] The recent availability of instrumentation for measuring mobility distributions of small (0.4–1.6 nm diameter) and intermediate (1.6–7.0 nm diameter) ions in the atmosphere provides another rich source of information for quantifying the role of ions in new particle formation [*Tammet*, 2002, 2003; *Fews et al.*, 2005]. Ion mobility distributions measured during nucleation events show the growth of small ions into the intermediate ion size range. Such data along with measurements of "total" (neutral plus charged) size distributions provide an independent approach for inferring the relative contributions of neutral nucleation and IIN to new particle formation.

[5] Small positive and negative ions are always present at ground level and are typically present in roughly equal concentrations [*Bricard*, 1966]. Direct qualitative evidence for IIN is the formation of intermediate ions of one polarity but not the other. This can occur when vapor condenses preferentially on small ions of one polarity because of the affinity of the vapor for that charge. Such charge asymmetry in the formation of intermediate ions was observed in Tahukse, Estonia [*Tammet et al.*, 1988, 1992]. Also, laboratory studies show that negative IIN occurs when particles are formed as a result of radioactive decay in mixtures of H_2O and SO_2 in N_2 [*Kim et al.*, 1997; *Wilhelm et al.*, 2004].

[6] Information about whether or not IIN occurred can also be obtained from measurements of the fraction of particles of a given size that are neutral, or negatively or positively charged. Nucleated particles will eventually achieve the stationary state charge distribution as they grow. However, if growth is sufficiently fast relative to charging (or neutralization) rates, differences between the actual and stationary-state charge fractions can provide information about the charge state of the nucleated particle and therefore about the nucleation process itself. Measurements in Tahukse, Estonia show that the measured fractions of charged particles in the nanoparticle size range were higher than the stationary state values during nucleation periods [*Hõrrak et al.*, 1998a; *Tamm et al.*, 2001; *Vana et al.*, 2004], and the trend becomes stronger as size decreases [*Tamm et al.*, 2001]. These observations suggest that IIN was occurring and that particles were neutralized by the attachment of small ions of the opposite polarity as they grew. Measurements in Hyytiälä, Finland showed that particles in the 3–5 nm size range were sometimes overcharged and sometimes undercharged relative to the expected stationary state charge during nucleation periods [*Laakso et al.*, 2004]. Three nucleation events in five consecutive days of measurements showed that negatively charged particles were in significant excess, suggesting that negative IIN occurred to some extent during these events.

[7] The ion generation rate limits the maximum particle production rate by IIN. *Eisele et al.* [2006] did a limiting case analysis and showed that typically observed ion generation rates during their measurement period cannot account for the observed particle formation in 3.0–5.5 nm range. The conclusion was also supported by *Yu*'s [2006] model, which accounts for the evaporation of charged and neutral clusters.

[8] This paper investigates the role of IIN in new particle formation events observed near ground level at a sampling site located near Boulder, Colorado. The measurements of mobility distributions of small and intermediate ions and the overall size distribution of particles were carried out. Our analysis proceeds in three steps. First we describe a theoretical analysis that identifies conditions under which nucleated particles "remember" their initial charge state. We then apply this approach to the Boulder data to show, qualitatively, whether the observed nanoparticle production is partially attributed to IIN or is dominated by nucleation onto neutral clusters. Finally we carry out quantitative analyses aimed at determining the fractional contribution of neutral, positive and negative IIN to new particle formation rates for each observed nucleation event.

2. Experiments

[9] Measurements of particle (3 nm to 5 μm) and positive and negative ion (0.4–6.3 nm) size distributions were carried out at the National Center for Atmospheric Research's Marshall Field Site located 5 miles southeast of Boulder, Colorado. Measurements were taken from mid March to the end of September during 2004 and from early May to the end of the October during 2005. During these months the production of ultrafine particles were observed for 70% of the measurement days. The frequency of the events did not strongly depend on the months that the measurements were taken. Aerosol size distributions were measured using a nanometer scanning mobility particle sizer (Nano-SMPS) system consisting of a nanometer differential mobility analyzer (Nano DMA; Model 3085, TSI, Inc.) [*Chen et al.*, 1998] coupled with an ultrafine condensation particle counter (UCPC; Model 3025, TSI, Inc.) [*Stolzenburg and McMurry*, 1991], a conventional SMPS consisting of a long-DMA (Model 3081, TSI, Inc.) [*Liu and Pui*, 1974] coupled with a CPC (Model 3010, TSI, Inc.), and an optical particle counter (OPC; LASAIR Model 1002, Particle Measuring Systems, Inc.). The size ranges measured by the Nano-SMPS, SMPS, and OPC are 3 to 34 nm, 21 to 266 nm, and 120 nm to 5 μm, respectively. Size distributions were measured every 5 min. A RH conditioner located upstream of the aerosol instrumentation maintained the relative humidity of the sampled aerosol at 40%. Prior to mobility analysis particles flowed through a ^{210}Po bipolar charger to produce stationary state charge distributions [*Adachi et al.*, 1983; *Hoppel and Frick*, 1986; *Wiedensohler et al.*, 1986]. The distribution function of total particles (neutral plus electrically charged) is measured with the SMPS [*Wang and Flagan*, 1990]. Size-dependent diffusion losses through each section of the sampling lines were estimated by using the Gormley-Kennedy equation [*Hinds*, 1999]. Penetrations of 3 nm particles through our sampling line with and without the RH conditioner are estimated to be 13% and 30%, respectively, and penetration efficiencies exceed 80% for particles above 20 nm particles.

[10] The mobility distributions of small and intermediate ions in 18 equal logarithmic intervals ranging from 6.3 to 0.5 $cm^2\ V^{-1}\ s^{-1}$ (0.4–6.3 nm) were measured using the Inclined Grid Mobility Analyzer (IGMA), which was developed by *Tammet* [2002, 2003]. The algorithm developed by *Tammet* [1995] was used to determine the size distribu-

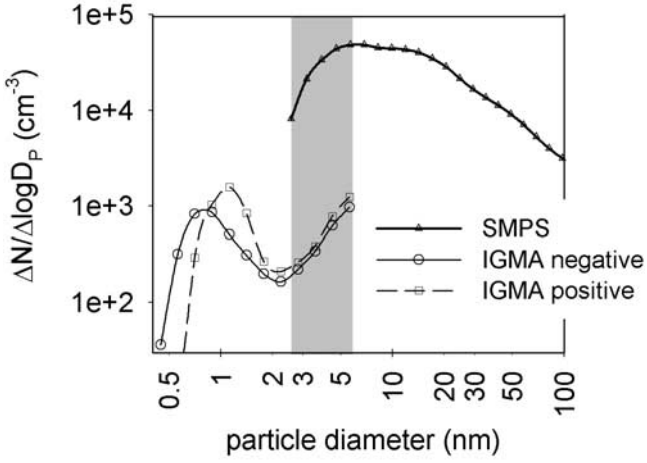

Figure 1. Typical particle size distribution measured by the scanning mobility particle sizer (SMPS) and the Inclined Grid Mobility Analyzer (IGMA) during the nucleation event on 1 June 2004. Particle size is defined as mass size [*Tammet*, 1995].

tions of ions. The concentration of ions sampled by the IGMA is calculated from the aerosol sampling flow rate and the ion current measured by the IGMA electrometer. Using a Model 8330 VelociCheck (TSI, Inc.), the inlet flow rate was found to be 2300 SLPM. The detection of charged particles within the IGMA is done by a sensitive electrometer, which can operate at high or low gain. The smallest and largest values of ion size distributions, $\Delta N/\Delta \log D_P$, that can be measured under the low and high gain modes are 10 cm^{-3} and 1×10^7 cm^{-3}. We carried out laboratory studies to evaluate the response of the IGMA to small ions of known mobility and concentration. Small positive ions, generated using the unipolar charger of *Chen and Pui* [1999], were used to evaluate the response of the IGMA to ions of known concentration; ion concentrations were measured using a Faraday Cage Electrometer (FCE) similar in design to that described by *Okuyama et al.* [1998]. Ion mobilities are determined by the voltage applied to the inclined grids. For mobility calibrations, 4.1 nm NaCl particles were generated using a nano-DMA that was set to operate at a mobility resolution of 20%.

[11] Figure 1 shows typical size distributions of small and intermediate ions (0.4–6.3 nm) and particles up to 100 nm in diameter measured during a nucleation event in Boulder. Note that the IGMA and the PSD data overlap from nominally 3.0–5.5 nm diameter enabling measurements of the charged fraction, $f_{overlap}^{(\pm 1)}$, in this size range. Owing to the much higher sensitivity of the IGMA compared with the SMPS, zero counts were often registered by the SMPS in some bins within the overlapping size range during low concentration periods, while the IGMA routinely detects charged particles. Therefore $f_{overlap}^{(\pm 1)}$ is only evaluated during the nucleation and growth periods in which particles in the overlapping size range are detected by the SMPS system at sufficiently high rate. The calculated total particle concentration in the overlapping size range is considered valid if its statistical uncertainty is below ~33% (9 counts). After data are corrected for transport losses the concentration corresponding to 9 counts is ~500 cm^{-3} when the SMPS measures a size distrib very 5 min.

[12] The major source of uncertainties in values of $f_{overlap}^{(\pm 1)}$ obtained using only SMPS and IGMA data is the transport loss through the SMPS system. The calculated diffusional transport losses through the SMPS sampling lines are uncertain. Recirculation or secondary flow can contribute to additional losses and are difficult to assess theoretically. In order to perform more accurate measurements of charged fractions, the dual-SMPS system shown in Figure 2 was deployed during 2005. The dual-SMPS system was designed to satisfy two measurement objectives: determination of charged fractions of atmospheric particles as small as 2.5 nm with improved accuracy, and comparison of the responses of the ultrafine Water CPC (UWCPC TSI 3786) and ultrafine butanol CPC (TSI 3025) to mobility-classified atmospheric particles. In this paper our use of the dual-SMPS data focuses on the measurement of charged fractions.

[13] Atmospheric aerosols are sampled into the dual-SMPS system at 2.0 LPM through either the ^{210}Po bipolar charger or the geometrically identical dummy neutralizer, depending on the direction chosen by the three way valve. The aerosol that passes through the bipolar charger reaches a stationary state charge distribution, while the aerosol that passes through the dummy neutralizer has the same charge state as the ambient air, assuming that charged and neutral particles are transported through the conducting sampling tubing with equal efficiency. Aerosols are classified by the two identical radial DMAs [*Zhang et al.*, 1995; *Zhang and Flagan* 1996] operated at equal flow rates. The polydisperse inlet and monodisperse outlet flows are set to 1.0 LPM and

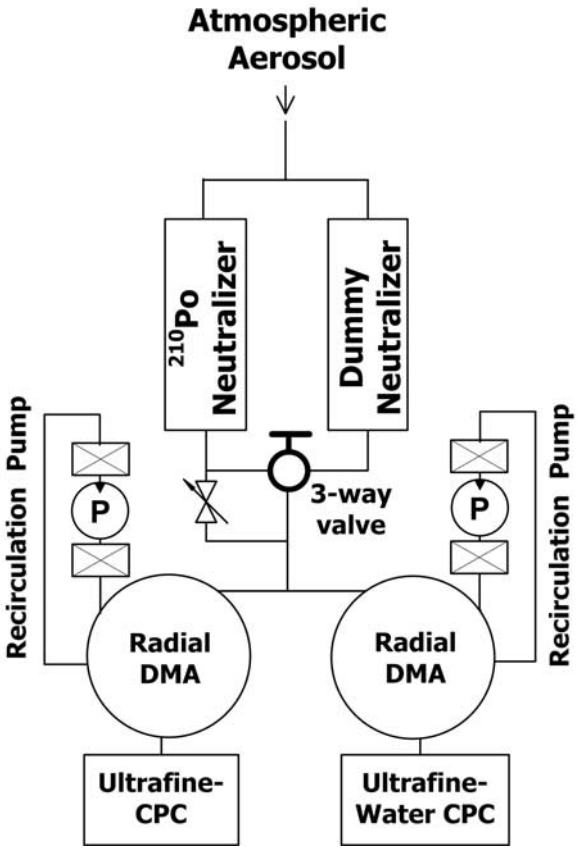

Figure 2. Schematic diagram of the dual-SMPS system.

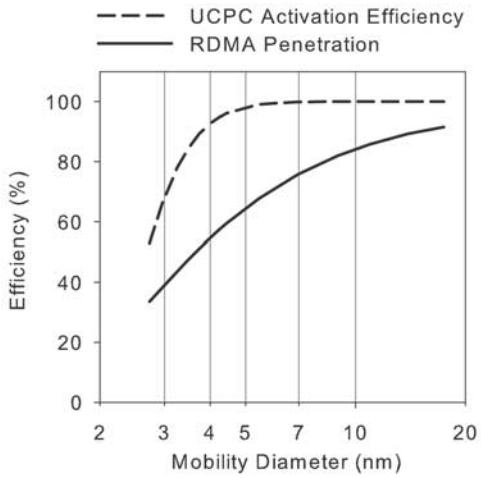

Figure 3. Ultrafine condensation particle counter (UCPC) counting efficiency and the radial differential mobility analyzer (RDMA) penetration efficiency obtained from a laboratory calibration using particles in the 2.7 to 17.4 nm diameter range.

the recirculating sheath flows are set to 7.5 LPM. The ultrafine CPC (UCPC) and ultrafine Water CPC (UWCPC TSI 3786) are used as detectors. The calibrated capillary flow rate of the UCPC and UWCPC are set at 0.63 $cm^3\ s^{-1}$ and 5.0 $cm^3\ s^{-1}$, respectively. The resulting count rate is about 8 times larger for the UWCPC, therefore the charge distribution measured by the UWCPC has significantly lower statistical noise than that measured by the UCPC. The two radial DMAs were checked for consistent performance by a TDMA technique [*Rader and McMurry*, 1986; *Stolzenburg*, 1988]. The dual SMPS operates in four modes: classification of positively and negatively charged particles sampled directly from the atmosphere and classification of positively and negatively charged particles from the ^{210}Po neutralizer. For each of these modes particles are counted with both the UCPC and the UWCPC. For each mode voltage was scanned upward in 2.5 min, therefore 10 min were used to complete measurements in all four modes of operation.

[14] Accurate measurements of charged fractions with this apparatus require accurate information on size-dependent sampling and detection efficiencies. We carried out laboratory measurements of detection efficiencies of the UCPC and transport efficiencies through the radial DMA for particles in the 2.7–17.4 nm diameter range. According to *Karlsson and Martinsson* [2003], the Gormley-Kennedy relation can be used to model size-dependent diffusional losses of ultrafine particles in DMAs. Following their approach, our experimentally obtained characteristic length was 179 cm. The activation efficiency of the butanol UCPC was also evaluated experimentally in the same size range using the inversion methodology described by *Stolzenburg and McMurry* [1991]. Figure 3 shows these radial DMA penetration and UCPC counting efficiencies. The activation efficiency of the WCPC was not measured in the laboratory prior to field sampling since previous work showed that near the minimum detectable size it is affected by the particle composition [*Biswas et al.*, 2005; *Hering et al.*, 2005]. It was found that the response of these two instruments to atmospheric particles was nearly identical for mobility-classified atmospheric particles during this sampling campaign [*Stolzenburg et al.*, 2006]. The following procedure was used to obtain more accurate values of $f_{overlap}^{(\pm1)}$ from the IGMA-SMPS measurements using information provided by the dual SMPS. First, we assume for reasons discussed previously that the measurements of $f_{overlap}^{(\pm1)}$ obtained with the dual SMPS are accurate. We also assume that the concentrations of positive and negative intermediate ions in the overlapping size range (3.0–5.5 nm diameter) are accurately measured by the IGMA, which samples directly from the atmosphere at a high rate. The following equation then provides the relationship between $f_{overlap}^{(\pm1)}$ measured by the dual SMPS system to the value measured with the IGMA-SMPS system:

$$f_{overlap}^{(\pm1)} = \frac{N_{Dual}^{(\pm1)}}{N_{Dual}^{Total}} = \kappa \frac{N_{IGMA}^{(\pm1)}}{N_{SMPS}^{Total}} \quad (1)$$

where $N_{Dual}^{(\pm1)}$ and N_{Dual}^{Total} are the charged and total concentrations in the overlap range measured by the dual-SMPS system, and $N_{IGMA}^{(\pm1)}$ and N_{SMPS}^{Total} are the charged and total concentrations in the overlap range measured by the IGMA and SMPS system, respectively. The factor κ is the concentration calibration factor of the SMPS system and is equal to the measured/true concentration of the total particles in the overlap range. We chose 4 days where good quality data were obtained with both the IGMA-SMPS and dual-SMPS systems, and evaluated κ for all distributions measured on those days. Figure 4 shows the frequency distribution of κ and its fitted lognormal distribution. The fitted lognormal distribution has a mean value of κ equal to 0.37 and geometric standard deviation 1.7. On the basis of these results we used a value of κ = 0.37 for analyzing data for the entire study period. As is explained below, however, we also examined the sensitivity of our results to the value of κ used when analyzing

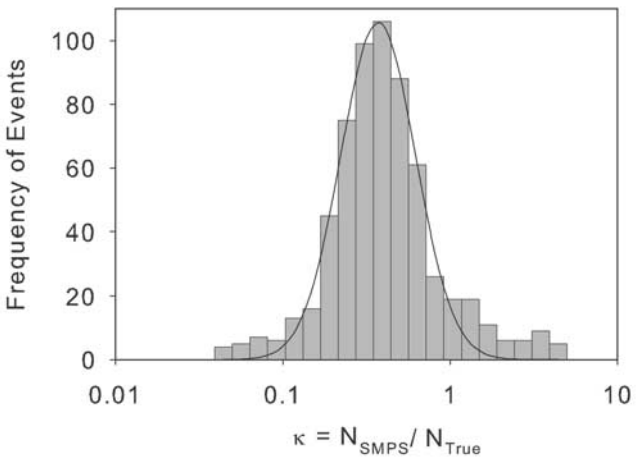

Figure 4. Frequency distribution of $\kappa = N_{SMPS}/N_{TRUE}$ obtained by analyzing 4 days of data for which we had simultaneous measurements of the IGMA, SMPS, and dual SMPS.

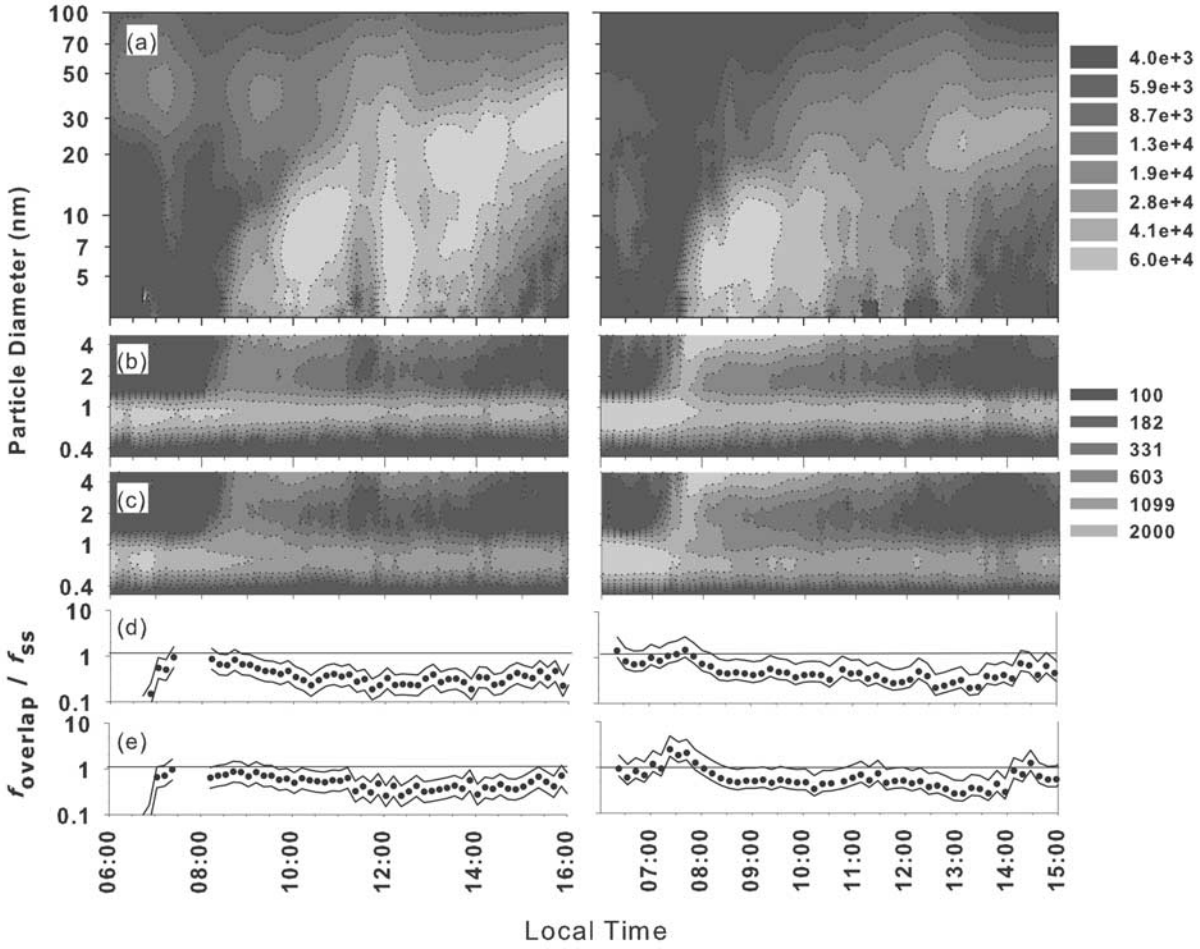

Figure 5. Measurements obtained during new particle formation events on (left) 15 May and (right) 1 June 2004. Contour plots of (a) the particle number distribution ($\Delta N/\Delta \log D_p$, cm^{-3}) and of (b) positive and (c) negative ion number distributions are shown. The ratios of observed to stationary state charged fractions in the IGMS-SMPS overlap range (3.0–5.5 nm) are shown for (d) positive and (e) negative particles. The dots and the lines above and below the dots are respectively obtained using the 50th, 84th, and 16th percentile values of κ from Figure 4.

the data, and found that our major conclusions are not significantly affected by uncertainties in κ.

[15] Figure 5 shows examples of data obtained during nucleation events on 15 May 2005 (left) and 1 June 2004 (right). Figure 5a shows contour plots of the particle size distributions of the total (charged plus neutral) particles, $\Delta N/\Delta \log D_P$, measured by the SMPS system. Figures 5b and 5c show the size distributions of small and intermediate positive and negative ions, respectively, measured by the IGMA. The distributions of small ions generally peaked below 1 nm, and they are almost always present in the atmosphere regardless of the weather and season. New particle formation usually started sometime between sunrise and noon and lasted for several hours. As is shown in Figures 5b and 5c, the concentration of the intermediate ions typically increases during these events. As shown in Figure 5a the particles that grew beyond the size range of the intermediate ions appear as total particles in the SMPS data. The growth continues for the rest of the day and the final size of the mode is usually between 10 and 100 nm. Figures 5d and 5e sho ratio of the measured charge fraction $f_{overlap}^{(\pm 1)}$, to the stationary state value [*Hoppel and Frick*, 1986; *Reischl et al.*, 1996]. Representative stationary state values were obtained by weighting the stationary state value of each size bin by the measured concentration of that bin. Values for this ratio are not shown when particle counts measured using the SMPS were too low to be statistically significant. The dots on Figures 5d and 5e show the measured values of this ratio for positive and negative particles assuming that $\kappa = 0.37$. The lines below and above the dots are obtained using the 16th and 84th percentile values of κ based on the distribution shown in Figure 4.

3. Results

3.1. Theoretical Analysis

[16] If particle growth rates are very slow or small ion concentrations are very high, particles will achieve a stationary state charge distribution by the time they reach the overlapping size range for the IGMA and SMPS regardless of their initial charge state. Under conditions pertinent to the atmosphere, however, particles often do not reach stationary

state distributions by the time they grow to this size range. In this section a simple theoretical analysis is performed to show conditions under which particles "remember" their nucleated charge state.

[17] The following set of population balance equations describes the growth of particles, their charging by the attachment of small ions, and their rates of loss by extramodal coagulation with preexisting particles under steady state. The equations were solved from mass sizes of 1 nm to 5.5 nm [*Tammet*, 1995] at linearly distributed size node i ranging form $i = 1$ to 101.

$$\frac{d}{dD_P}\left(n_i^{(0)}\frac{dD_P^{(0)}}{dt}\bigg|_i\right) = -\Gamma_i^{(0)}n_i^{(0)} - \beta_i^{(+,0)}c^+n_i^{(0)} - \beta_i^{(-,0)}c^-n_i^{(0)} + \beta_i^{(-,+1)}c^-n_i^{(+1)} + \beta_i^{(+,-1)}c^+n_i^{(-1)} \quad (2)$$

$$\frac{d}{dD_P}\left(n_i^{(+1)}\frac{dD_P^{(+1)}}{dt}\bigg|_i\right) = -\Gamma_i^{(+1)}n_i^{(+1)} + \beta_i^{(+,0)}c^+n_i^{(0)} - \beta_i^{(-,+1)}c^-n_i^{(+1)} \quad (3)$$

$$\frac{d}{dD_P}\left(n_i^{(-1)}\frac{dD_P^{(-1)}}{dt}\bigg|_i\right) = -\Gamma_i^{(-1)}n_i^{(-1)} + \beta_i^{(-,0)}c^-n_i^{(0)} - \beta_i^{(+,-1)}c^+n_i^{(-1)} \quad (4)$$

In the above equations, $n_i^{(q)}$ is the number distribution, $dN^{(q)}/dD_P$ of particles with charge state q at size i. Concentrations of positive and negative small ±ions, $c^{\pm}$, are measured by the IGMA. The ion-aerosol attachment coefficients between ±ions and particles with charge state q at size i, $\beta_i^{(\pm,q)}$, were calculated by using the limiting sphere theory of *Fuchs* [1963] as described by *Reischl et al.* [1996]. The condensational growth rates of particles with charge state q at size i, $dD_P^{(q)}/dt|_i$ was calculated by the following expression.

$$\frac{dD_P}{dt}\bigg|_i^{(q)} = \frac{dD_P}{dt}\bigg|_\infty \cdot RM_i \cdot \tilde{\Omega}_i^{(q)} \quad (5)$$

where $dD_P/dt|_\infty$ is the free molecular regime growth rate given by

$$\frac{dD_P}{dt}\bigg|_\infty = \frac{1}{2}\frac{m_{vap}}{\rho_{vap}}v_{vap}c_{vap} \quad (6)$$

where m_{vap}, ρ_{vap}, v_{vap}, and c_{vap} are molecular mass, density, mean thermal speed, and the concentration of the vapor, respectively. Using the terminology of *Tammet and Kulmala* [2005] we refer to $dD_P/dt|_\infty$ as the plain Knudsen growth rate and consider it to be independent of size in this analysis. The factor RM_i is the enhancement in collision between the condensing vapor and growing particle at size i due to their relative motion:

$$RM_i = \left(1 + \frac{d_{vap}}{D_P|_i}\right)^2\sqrt{1 + \left(\frac{d_{vap}}{D_P|_i}\right)^3} \quad (7)$$

where d_{vap} is the diam a vapor molecule.

[18] The term $\tilde{\Omega}_i^{(q)}$ is the condensation enhancement factor of particles with charge state q at size i due to the electrostatic potential between a charged nanoparticle and permanent and induced dipole moments of the condensing vapor [*Nadykto and Yu*, 2003; *Tammet and Kulmala*, 2005] which can be calculated if the composition of the condensing vapor is known. In this study, the condensing vapor is assumed to be H_2SO_4, and the dimensionless collision integral of *Tammet and Kulmala* [2005] was used to calculate $\tilde{\Omega}_i^{(q)}$. Furthermore, we assumed that the condensing vapor has no chemical affinity toward charged particles of specific polarity; therefore $\tilde{\Omega}_i^{(q)}$ is independent of polarity ($dD_P^{(1)}/dt = dD_P^{(-1)}/dt$). Finally, the effect of evaporation was not included in the collision integral in this study.

[19] The laboratory study of [*Hanson and Eisele*, 2002] suggested that $NH_3 \cdot (H_2SO_4)_2 \cdot (H_2O)_y$ is likely to be the critical cluster for neutral nucleation at their laboratory condition (270 K and $[H_2SO_4] = 2 \times 10^9$ cm^{-3}), which gives a critical size of 0.7–0.8 nm. The temperature and $[H_2SO_4]$ during our observed nucleation period ranged from 274–300 K and $0.1–4 \times 10^7$ cm^{-3}, respectively, suggesting that the critical size based on ternary nucleation theory is larger than 1 nm. However, the mechanism by which critical nuclei are formed is not well understood. It follows that evaporation may or may not be significant at 1 nm. On the other hand, theoretical studies showed that the dissociation rates of $HSO_4^- \cdot (H_2SO_4)_x \cdot (H_2O)_y$ are significant at $x = 2$ and perhaps for cluster sizes above this [*Lovejoy et al.*, 2004; *Eisele et al.*, 2006], suggesting, that the evaporation rate may or may not be significant at 1 nm during IIN.

[20] The variable $\Gamma_i^{(q)}$ is the condensation sink to preexisting particles (time^{-1}) and is calculated from SMPS data using the following expression:

$$\Gamma_i^{(q)} = \sum_p^{\substack{\text{charge}\\ \text{states}}}\sum_j^{\substack{\text{SMPS}\\ \text{size bins}}}\frac{\beta_{i,j}\Delta N_j^{(p)}}{W_{i,j}^{(q,p)}} \quad (8)$$

where $\beta_{i,j}$ is the coagulation coefficient between neutral particles of size $D_P|_i$ and $D_P|_j$ [*Fuchs*, 1964; *Tammet and Kulmala* 2005] and $\Delta N_j^{(p)}$ is the concentration of particles in the jth size bin of the SMPS data with charge state p. For sizes up to 50 nm, charged fractions were calculated with the limiting sphere theory of Fuchs [*Fuchs* 1963; *Reischl et al.*, 1996], while the theory of *Gunn* [1954] was used for particles larger than this [*Wiedensohler*, 1988]. The factor, $W_{i,j}^{(q,p)}$ accounts for the increase and decrease in coagulation rates because of charge [*Seinfeld and Pandis*, 1998]. Charge states up to $p = \pm 5$ were considered. In evaluating $W_{i,j}^{(q,p)}$, the electrostatic potential between the two conductive particles $\Phi_{i,j}^{(q,p)}$ was calculated by using the following simplified form:

$$\Phi_{i,j}^{(q,p)}(r) = \frac{e^2}{4\pi\varepsilon_0}\left(\frac{qp}{r} - \left|\frac{qr_j^3}{2r^2\left(r^2 - r_j^2\right)} - \frac{pr_i^3}{2r^2(r^2 - r_i^2)}\right|\right) \quad (9)$$

where r is the distance between the centers of two particles with radius r_i and r_j. The first and second terms are the potential due to coulomb and image forces, assuming that particles can be treated as point charges. This approach neglects higher-order image charges, such as are described by equations (30)–(34) of *Laakso et al.* [2002]. We found

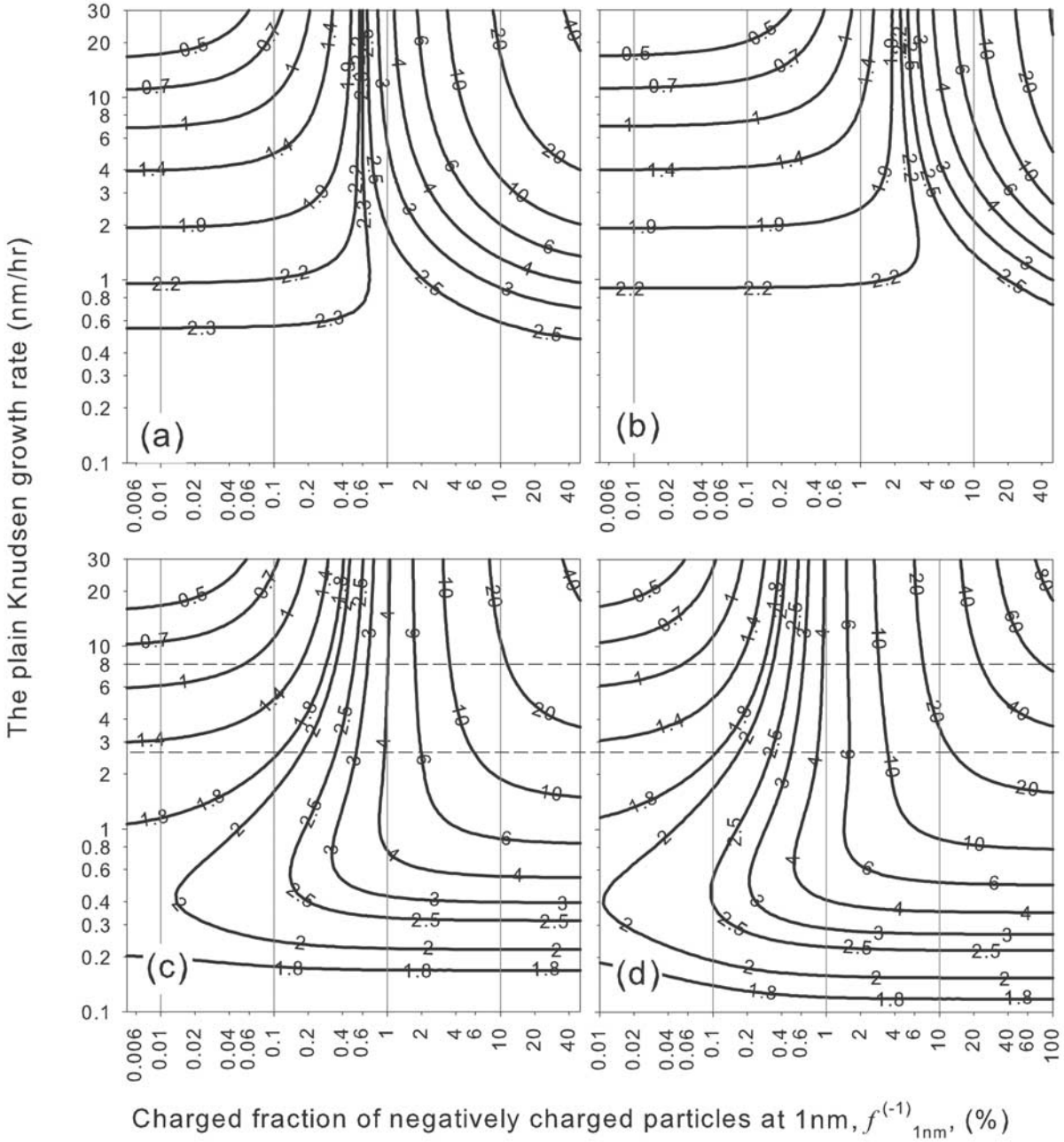

Figure 6. Contour plots of steady state charged fractions of negatively charged particles in the overlapping size range ($f^{(-1)}_{overlap}$, in %) as a function of the plain Knudsen growth rate and initial charged fraction of negative particles at 1 nm, $f^{(-1)}_{1nm}$. (a and b) Cases comparing the effect of charge dipole interactions but with no condensation sink. (c and d) Cases including the effect of condensation sink $\Gamma_i^{(q)}$ and comparing the difference between bipolar and unipolar cases. The differences in assumptions made for each case are shown in Table 1.

that these higher-order corrections only change $\Gamma_i^{(q)}$ by about 0.5% for our application.

[21] For the illustrative calculations reported in this section, positive and negative small ion concentrations are assumed equal to 800 cm^{-3} with average mobilities of 1.75 $cm^2\ V^{-1}\ s^{-1}$ for both polarities. A particle size distribution of the preexisting particles that has a Fuchs surface area [*McMurry et al.*, 2000, 2005] of 81 $\mu m^2\ cm^{-3}$ was chosen. These values are representative of conditions observed in Boulder. In order to examine the competition between growth and charging/recombination the relative motion effect in growth rate (RM_i) in equation (5) is set to unity because the Fuchs limiting sphere approach does not account for the relative motion between small ions and particles.

[22] At this point it is worth clarifying terminology for two different steady state charged fractions. In the absence

Table 1. Differences in the Assumptions for the Cases Shown in Figure 6

Cases	Charged Fraction at 1 nm, $f_{1nm}^{(\pm1)}$	Charge-Dipole Interactions, $\tilde{\Omega}_i^{(q)}$	Condensation Sink, $\Gamma_i^{(q)}$
Figure 6a	$f_{1nm}^{(+1)} = f_{1nm}^{(-1)}$	included	not included
Figure 6b	$f_{1nm}^{(+1)} = f_{1nm}^{(-1)}$	not included	not included
Figure 6c	$f_{1nm}^{(+1)} = f_{1nm}^{(-1)}$	included	included
Figure 6d	$f_{1nm}^{(+1)} = 0$	included	included

of particle growth the charged fraction is referred to as the "stationary state" charged fraction following the nomenclature used by *Fuchs* [1963]. When particle growth is included the charged fractions are referred to as "steady state."

[23] Figures 6a–6d show contour plots of the steady state charged fraction of negatively charged particles in the overlap range, $f_{overlap}^{(-1)}$, as a function of the plain Knudsen growth rate and the initial charged fraction of negatively charged particles at 1 nm, $f_{1nm}^{(-1)}$. The differences in the assumptions made for each case are shown in Table 1.

[24] The cases shown in Figures 6a and 6b compare the effect of charge dipole interactions but with no condensation sink. For cases where charge-enhanced growth is not taken into account (Figure 6b), contours of $f_{overlap}^{(-1)}$ asymptotically approaches $f_{1nm}^{(-1)}$ as the growth rate increases. On the other hand, if the charge enhanced growth is taken into account (Figure 6a), $f_{overlap}^{(-1)}$ exceeds $f_{1nm}^{(-1)}$ at higher growth rates. At growth rates lower than $\sim$0.4 nm h^{-1}, $f_{overlap}^{(-1)}$ is essentially independent of $f_{1nm}^{(-1)}$ indicating that the stationary state is reached by the time particles reach the overlapping size range, and no information about the charge state of the nucleated particles can be inferred. For growth rates above $\sim$0.6 nm h^{-1} Figures 6a and 6b are separated into two regions by the vertical contour lines in the neighborhood of the stationary state value in the overlap region (about 2.3–2.4%). To the left of this line $f_{overlap}^{(-1)}$ decreases as the growth rate increases since the charging of neutral particles by negative ions is the dominant process during growth. Since the nucleated particles were initially almost all neutral, the vapor predominantly nucleated onto neutral clusters. On the other hand, to the right of the dividing line, $f_{overlap}^{(-1)}$ increases as the growth rate increases because of recombination. Since a significant fraction of nucleated particles was initially charged, ion-induced nucleation contributes to new particle formation under these conditions. The ability to observe the dominance of either electrical charging or recombination is another method to characterize the nucleation process.

[25] The cases in Figures 6c and 6d include the effect of condensation sink $\Gamma_i^{(q)}$. For case shown in Figure 6c the both positively and negatively charged particles are present at 1 nm, while for the case in Figure 6d only negatively charged particles were present. Although not shown here, the effect of the condensation sink on $f_{overlap}^{(-1)}$ is negligible if the electrostatic effects between the growing nanoparticles and preexisting particles are not included ($W_{i,j}^{(q,p)} = 1$). The electrostatic interaction increases the depletion rate of the charged particles therefore decreases $f_{overlap}^{(-1)}$. For our measurements in Boulder, the growth rates ranged from 2.5 to 8 nm h^{-1} as shown by the dotted lines on Figures 6c and 6d. In this range of growth rate, $f_{overlap}^{(-1)}$ is sensitive to $f_{1nm}^{(-1)}$ for both the bipolar (Figure 6c) and the unipolar cases (Figure 6d) for a wide of $f_{1nm}^{(-1)}$, which indicates that particles in the overlapping size range of the IGMA and SMPS should remember their initial charge state.

3.2. Qualitative Analysis

3.2.1. Charged Fraction Measured by the Dual-SMPS System

[26] The theoretical analysis in the previous section concluded that freshly nucleated particles in the overlapping size range (3.0–5.5 nm) remember their initial charge state over the range of growth rates typically observed in this study. In this section actual charged fractions measured by the dual SMPS before, during, and after the nucleation event are shown for one representative case. The analysis is extended to all data collected between 15 June 2005 and 27 October 2005 to draw inferences about the dominant nucleation process during this period.

[27] Figure 7 shows data for charged fractions observed on 7 October 2005 in three size ranges11.2–24.5 nm (Figure 7b), 5.1–11.2 nm (Figure 7c) and 2.4–5.1 nm (Figure 7d), normalized by the stationary state charged fraction. Because counting rates obtained with the UWCPC are nearly an order of magnitude higher than those obtained with the UCPC, we used data from that instrument to obtain charged fraction measurements for particles down to 2.5 nm. Note that during the period when freshly nucleated particles were present, the measured fraction of both positive and negative particles in the 2.5–5.1 nm and 5.1–11.2 nm size ranges were below the stationary state value; therefore the nucleated particles are initially almost all neutral and they are acquiring charge as they grow.

[28] Using the data from 15 June to 27 October, representative charged fractions during nucleation periods were calculated for each day in five different size intervals. The criterion used to identify a "nucleation period" was that the concentration of particles in the size interval is at least 5 times the baseline values, and this elevated concentration persists for more than 30 min during daytime. Baseline concentrations were evaluated from data collected between midnight and 5 am, when nucleation was never observed. Figure 8 shows the ratio of the average and standard deviation of charged fraction during nucleation periods normalized by stationary state values. Note that the charged fractions during the nucleation periods are significantly below the stationary state values and the trend becomes stronger as size decreases. The freshly nucleated particles are significantly undercharged and approach the stationary value as they grow. This observation provides clear qualitative evidence that the nucleation events observed during 15 June to 27 October 2005 are dominated by neutral nucleation.

3.2.2. Particle Current of the Intermediate Ions

[29] As mentioned above, the ability to observe the dominance of either electrical charging or recombination is another method to characterize the nucleation process. In

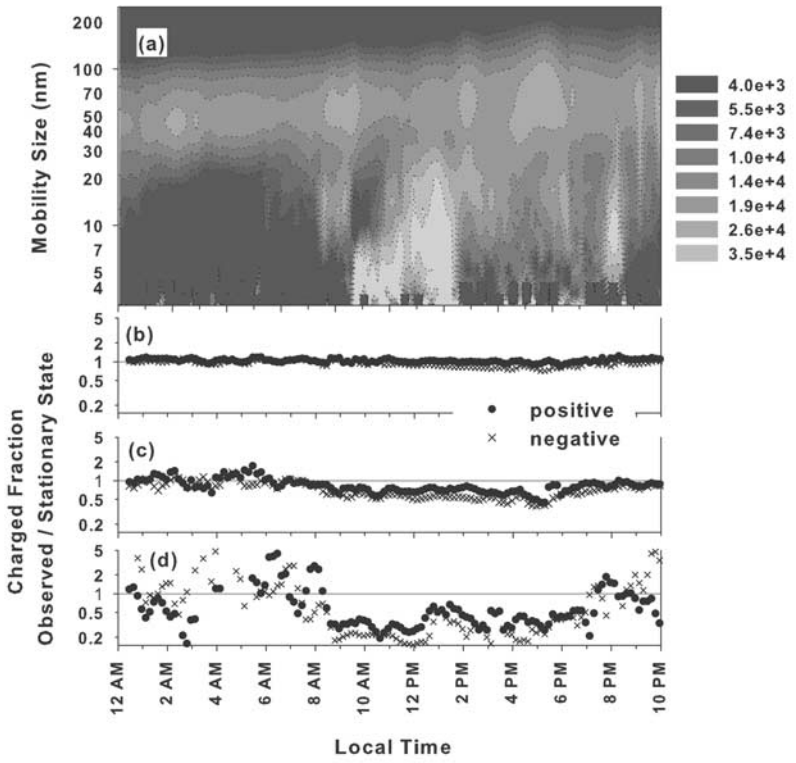

Figure 7. Measurements obtained during the new particle formation event on 7 October 2005. (a) Contour plots of the particle number distribution ($\Delta N/\Delta \log D_p$, cm^{-3}) are shown. The dimensionless charged fraction, defined as the ratio of the measured to the stationary state charged fractions, is shown for three size ranges: (b) 11.2–24.5, (c) 5.1–11.2, and (d) 2.4–5.1.

fact, it is possible to qualitatively infer, with a minimum of assumptions, whether IIN contributed to particle formation by analyzing the current of particles past a given size of intermediate ions. The advantage of this approach is that it does not require measurements of charged fraction, which is often limited by the low number of counts obtained by the SMPS system in 3–5.5 nm range.

[30] When size distributions are affected only by particle growth, the evolution of the size distribution is determined by the following form of the general dynamic equation [*Friedlander*, 2000]:

$$\frac{\partial n}{\partial t} + \frac{\partial J}{\partial D_P} = 0 \tag{10}$$

where n is the particle number distribution, dN/dD_P and J is the particle current, which can be approximated as [*Friedlander*, 2000]:

$$J \cong n \frac{dD_P}{dt} \tag{11}$$

where dD_P/dt is the particle growth rate. Equation (10) can be solved by the method of characteristics. If dD_P/dt depends only on size but not on time, it then follows that J does not vary with time as particles grow. If there were a source or sink of particles, however, then the RHS of equation (10) would be nonzero. If the RHS were negative, indicating a particle sink, then J would decrease as the diameter of the particle population grew, while J would increase if sources were dominant. In this section we show how such trends in J provide another qualitative source of information regarding the nucleation process.

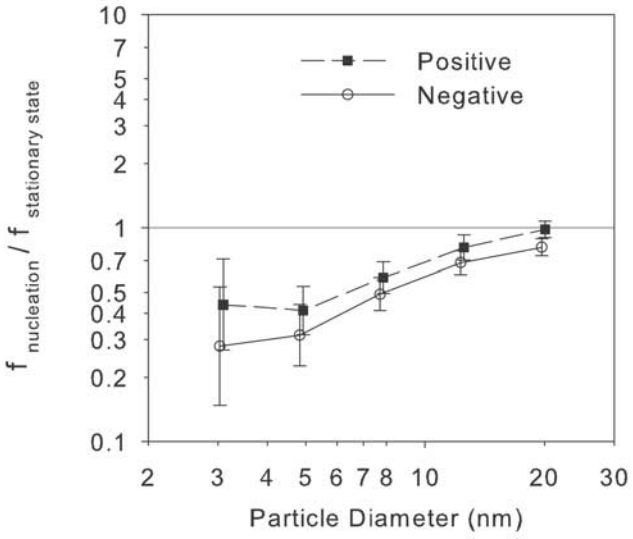

Figure 8. Ratio of the average charged fraction during the nucleation hours to the stationary state value for all new particle formation events observed from 15 June 2005 through 27 October 2005. The ultrafine water condensation particle counter was the SMPS detector for all of these data.

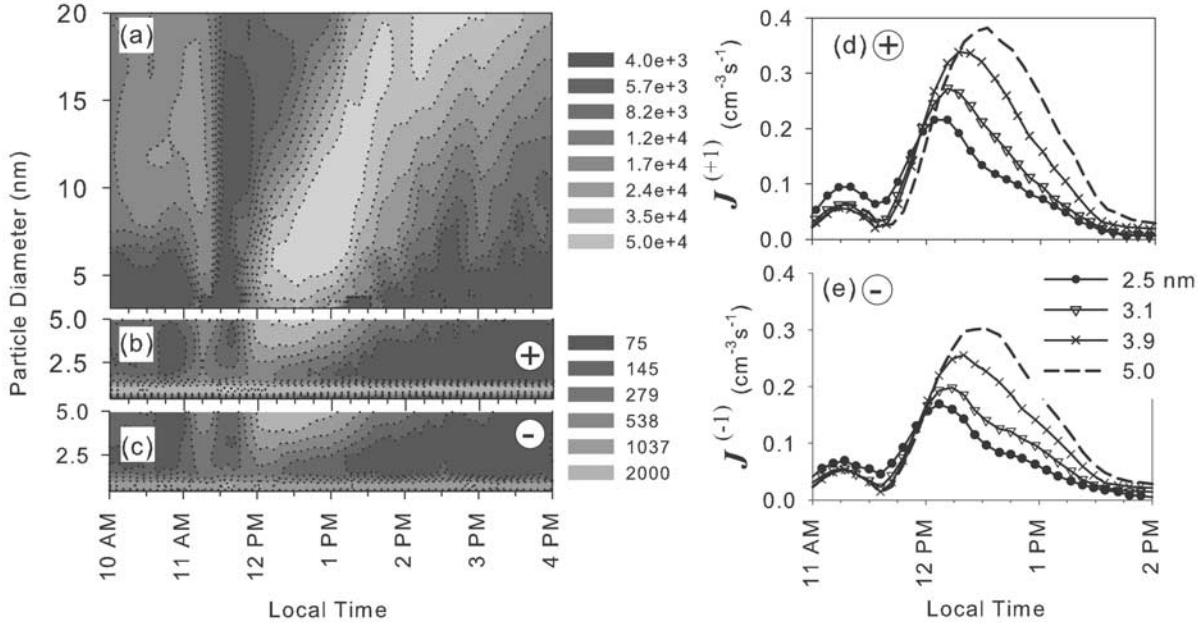

Figure 9. Measurements obtained during the new particle formation event on 7 May 2004. Number distributions ($\Delta N/\Delta \log D_p$, cm^{-3}) of (a) total (SMPS), (b) positive (IGMA), and (c) negative (IGMA) particles are shown. $J^{(\pm 1)}$ (cm^{-3} s^{-1}) for (d) positive and (e) negative intermediate ions versus time are shown.

[31] Equations (5) and (11) can be used to estimate the particle current of intermediate ions at each IGMA size bin k as follows:

$$J_k^{(\pm 1)} \cong \left.\frac{\Delta N}{\Delta D_P}\right|_k^{(\pm 1)} \cdot \left.\frac{dD_P}{dt}\right|_\infty \cdot RM_k \cdot \tilde{\Omega}_k^{(\pm 1)} \qquad (12)$$

The IGMA measures the particle number distribution, $\Delta N/\Delta D_P$, for particles that contain a single positive or negative charge. Furthermore, SMPS data for particles in the free molecule regime show that particle growth rates are typically approximately independent of size and time during a given event. The effect of charge-enhanced growth in this size range ($D_p > 3.5$ nm) is insignificant since the total population is dominated by neutral particles. We interpret the measured growth rates of total particles as the plain Knudsen growth rate in our observed nucleation events. The plain Knudsen growth rate was calculated from the SMPS data in the size range where the growing mode is clearly observable. Observed modal growth rates are affected by both condensation and coagulation [*Stolzenburg et al.*, 2005] therefore are corrected for the effect of coagulation.

[32] Figure 9 shows the nucleation event observed on 7 May 2004. Figures 9a–9c are contour plots similar to those shown in Figure 5 with the exception that a linear scale is used on the vertical axis. Figures 9d and 9e show values of $J^{(\pm 1)}$ versus time for positive and negative particles of four sizes. Note that the peaks of the $J^{(\pm 1)}$ curves shift to higher values with increasing particle size, which is evidence that charged particles in the indicated size ranges were produced by the attachment of small ions to relatively abundant neutral particles that were formed during this event.

[33] Figure 10 shows observations from 13 June 2004. In this case, the peak value of $J^{(\pm 1)}$ decreases for both positive and negative ions, indicating that significant depletion occurred as particles grew. Processes that could lead to depletion are recombination with small ions and coagulation with preexisting particles. The relative importance of these two depletion mechanisms for this period was compared theoretically. The results showed the rate of depletion by recombination exceeded the scavenging rate for the size above 2 nm. Therefore the observed decrease in particle current for the intermediate ions indicates that the nucleated particles are electrically neutralized as they grow, and the charged fraction of the nucleated particles was significantly above the stationary state value. These results are consistent with the hypothesis that both positive and negative IIN likely contributed to new particle formation on this occasion. This analysis provides no quantitative information on the extent to which IIN contributed to new particle formation, however.

[34] Data from 8 August 2004 are shown in Figure 11. Additionally, Figure 11d shows the concentration ratio of negative to positive particles measured by the IGMA. The degree of asymmetry is especially high (>3) when the nucleated particles first appear in the size range of the intermediate ions, but this ratio approaches unity as size and time increase beyond this point. Note also that trends in $J^{(\pm 1)}$ for positive and negative particles in Figures 11e and 11f show that electrical charging and recombination are the respectively dominant processes during growth. This indicates the rate of negative IIN exceeded the rate of positive IIN on this day. Such charge asymmetries were observed in only three out of 203 new particle formation events in this study. In two of these cases negative IIN was dominant, while in the third case positive IIN was dominant. One

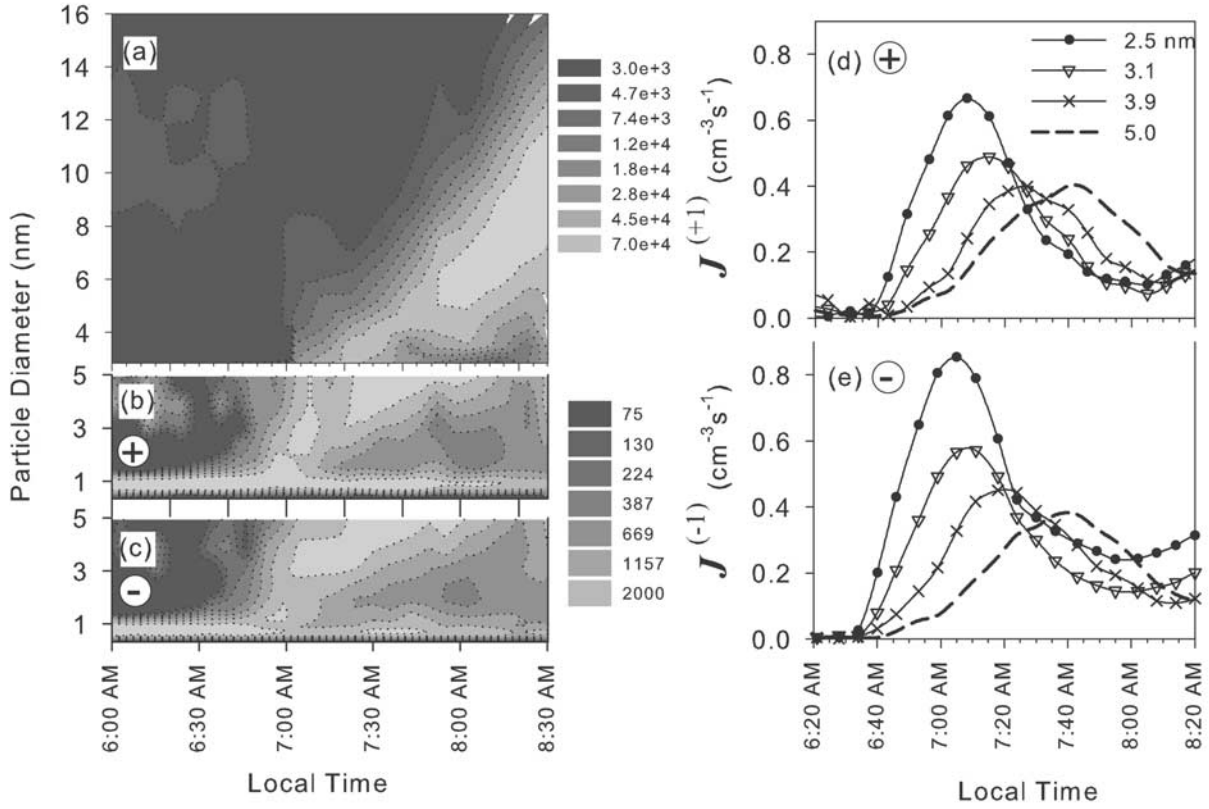

Figure 10. Measurements obtained during the new particle formation event on 13 June 2004. Number distributions ($\Delta N/\Delta \log D_p$, cm^{-3}) of (a) total (SMPS), (b) positive (IGMA), and (c) negative (IGMA) particles are shown. $J^{(\pm 1)}$ (cm^{-3} s^{-1}) for (d) positive and (e) negative intermediate ions versus time is shown.

possible process that could lead to negative IIN is the affinity of sulfuric acid vapor toward negative ions [*Lovejoy et al.*, 2004; *Wilhelm et al.*, 2004; *Eisele et al.*, 2006].

[35] There may be processes that were not considered in this analyses that could lead to asymmetries in concentrations of positive and negative intermediate ions. For example, positive and negative ions have distinctly different compositions, as reflected by their differing mobilities. Chemical affinities between the nucleated particles and positive or negative ions might cause the particles to combine preferentially with ions of one polarity. Including such effects requires reevaluating the attachment coefficient $\beta_i^{(\pm,q)}$. Similarly, polarity-dependent chemical affinity between the condensing vapor and nucleated charged particles might cause the charged particles of one polarity to grow faster than the other. Accounting for this effect requires reevaluating the nondimensional collision integral $\tilde{\Omega}_i^{(q)}$.

3.3. Quantitative Analysis

[36] The above qualitative analyses enable us to determine whether IIN contributed to new particle formation in a given observed nucleation event but did not quantify the relative contributions of neutral nucleation and IIN. In this section, an analysis tool similar to that described by *Tammet and Kulmala* [2005] is used to estimate the relative contributions of ion induced and neutral species nucleation for these events.

[37] The key inputs to the analysis tool are: the plain Knudsen growth rate, the electrical mobility and concentration of the small positive and negative ions, the particle size distribution of the preexisting and freshly nucleated particles, and the charged fraction in the overlapping size range of the SMPS and IGMA. Except for the plain Knudsen growth rate all the input parameters are calculated by averaging measurements made during a nucleation event, beginning when concentrations in the overlapping size range started to increase, and ending when concentrations of the total particles in the overlapping size range started to decay. Using the time averaged distribution in the overlapping size range, $\bar{n}_{\mathrm{overlap}}$, the charged fractions are obtained by $\bar{f}^{(\pm 1)}_{\mathrm{overlap}} = \bar{n}^{(\pm 1)}_{\mathrm{overlap}}/\bar{n}^{\mathrm{total}}_{\mathrm{overlap}}$.

[38] We solve equations (2)–(4) by a "shooting technique" to determine the concentration of 1 nm particles of each charge state ($n^{(q)}_{1\mathrm{nm}}$, $q = -1, 0, +1$), that yields $\bar{f}^{(\pm 1)}_{\mathrm{overlap}}$ and $\bar{n}_{\mathrm{overlap}}$ after condensational growth and collisions with small ions and preexisting particles. After this solution is obtained, the total particle current at 1 nm, $J^{\mathrm{total}}_{1\mathrm{nm}}$, and the fractional contribution of IIN to nucleation rates, $\eta^{(\pm 1)}_{1\mathrm{nm}}$, are calculated as follows.

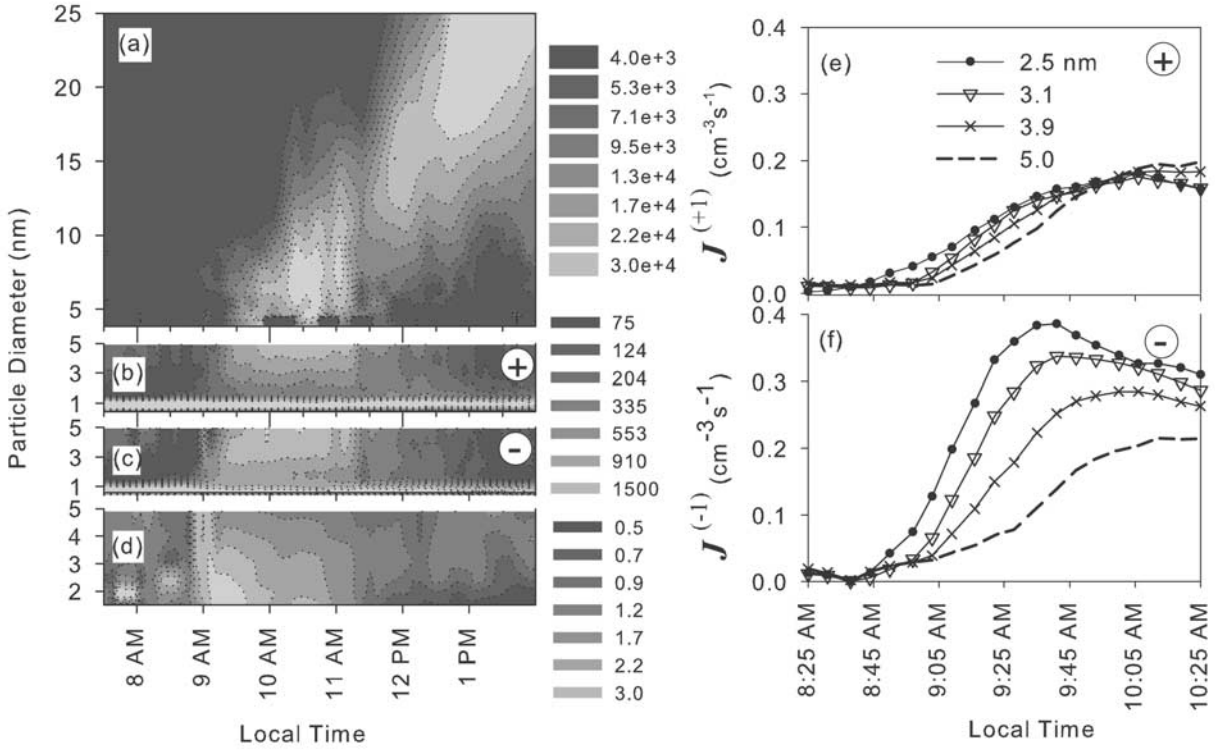

Figure 11. Measurements obtained during the new particle formation event on 8 August 2004. Number distributions ($\Delta N/\Delta \log D_p$, cm^{-3}) of (a) total (SMPS), (b) positive (IGMA), and (c) negative (IGMA) particles and (d) the ratio of positive to negative distribution functions are shown. $J^{(\pm 1)}$ (cm^{-3} s^{-1}) for (e) positive and (f) negative intermediate ions versus time is shown.

$$J_{1nm}^{(q)} = n_{1nm}^{(q)} \left. \frac{dD_p^{(q)}}{dt} \right|_{1nm} \quad (13)$$

$$J_{1nm}^{total} = \sum_q J_{1nm}^{(q)} \quad (14)$$

$$\eta_{1nm}^{(\pm 1)} = J_{1nm}^{(\pm 1)} / J_{1nm}^{total} \quad (15)$$

The plain Knudsen growth rate, $dD_P/dt|_\infty$, was calculated from the SMPS data in the size range where the growing mode is clearly observable. As was mentioned above, our observations show that $dD_P/dt|_\infty$ is approximately independent of both size and time. To obtain the initial guesses of $n_{1nm}^{(q)}$, n_{1nm}^{total} was first obtained by equation A7 of *McMurry et al.* [2005]:

$$\ln\left(\frac{n_1^{total}}{n_0^{total}}\right) = -\frac{1}{2}\frac{A_{Fuchs}}{dD_P/dt|_\infty}\left[\frac{48 k_B T}{\pi^2 \rho}\right]^{1/2} \cdot \left[D_{P0}^{-1/2} - D_{P1}^{-1/2}\right] \quad (16)$$

where the subscript 0 indicates the initial size (1 nm in this work), 1 a representative size in the overlapping size range (taken to be 4.2 nm in this study), and ρ particle density. Equation (16) is the analytical solution of the governing equation under constant growth rate ($dD_P/dt = dD_P/dt|_\infty$) and scavenging by the preexisting aerosol surface area, A_{Fuchs}. Next, initial guesses for $n_{1nm}^{(q)}$ were made by assuming $n_{1nm}^{(q)} = n_{1nm}^{total} \cdot f_{1nm}^{(q)}$, where $f_{1nm}^{(q)}$ is the stationary state charge fraction.

[39] The procedure outlined above was used to determine contributions of positive and negative IIN for 19 nucleation events from which growth rates could be obtained from the SMPS data. Figure 12 shows frequency distributions of the fractional contributions of positive and negative IIN estimated for these events. Table 2 lists some meteorological, aerosol, and ion parameters that were observed during these nucleation periods. The geometric average and standard deviation of $\eta_{1nm}^{(\pm 1)}$ for these frequency distributions are shown in Table 3 for the 50th and 84th percentile values of κ in equation (1). Note that the overall contribution of IIN is not seriously affected by the uncertainty in the value of κ.

[40] On the basis of these results we conclude that IIN did not contribute significantly to particle production during this study. This result is consistent with the recent measurement of sulfuric acid ion clusters at the same sampling site by *Eisele et al.* [2006]. They did not observe sulfuric acid ion clusters $H_2SO_4^- \cdot (H_2SO_4)_x \cdot (H_2O)_y$, for values of x greater than 2 during three nucleation events and concluded that negative ion clusters did not grow by the IIN pathway. The conclusion is also consistent with recent numerical models for IIN [*Lovejoy et al.*, 2004; *Yu*, 2006]. The concentration of H_2SO_4 was measured during daytime for 13 days during September 2004. The concentration ranged from 1×10^6 to 4×10^7 cm^{-3} and the average was around

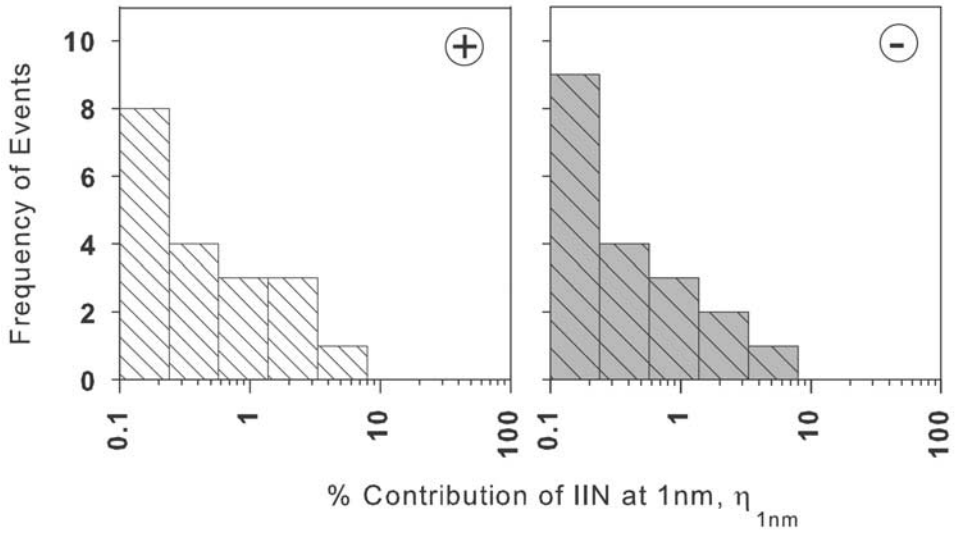

Figure 12. Frequency distribution of the fractional contributions of (left) positive and (right) negative IIN during the 19 nucleation events that were analyzed for data collected from March 2004 to May 2005.

1.5×10^7. The temperature and relative humidity ranged from 1.0–26°C and 14–77% during the nucleation events. The model shows that IIN is unlikely the dominant nucleation mechanism for the observed range of temperature, RH, and H_2SO_4.

[41] In our analysis the effect of evaporation was neglected. Two limiting cases can be used to assess the possible bias on our conclusion by not including evaporation. If the evaporation occurs to a significant extent as neutral particles are formed, a higher nucleation rate of neutral particles would be needed to achieve the observed concentration of the total particles in the overlapping size range. Therefore our main conclusion would not be affected. On the other hand, slower growth rates caused by a strong effect of evaporation would cause the charged fraction to reach the stationary state value before the particles reach the overlapping size range. However, as already shown in Figures 7 and 8, our data clearly show that charge fractions of the smallest particles are well below the stationary state values. If growth rates were slower than we assumed because of evaporation, neutral nucleation would have had to be even more dominant.

[42] The underlying assumption of this analysis is that nonsteady behavior of the actual nucleation events could be modeled as steady state processes (i.e., $J_{1nm} \cong$ constant). In order to examine the sensitivity of our results to this assumption, additional analyses were performed. The analysis showed that including the nonsteady effects led to changes in $\eta_{1nm}^{(\pm1)}$ and J_{1nm}^{total} less than 10%; therefore reasonably accurate solutions can be obtained using the steady state assumption.

4. Conclusion

[43] The role of IIN was investigated for new particle formation events observed near ground level at a sampling site located near Boulder, Colorado. The conclusions are based on measurement obility distribution of small and intermediate ions (0.4–6.3 nm), the size distribution of the total particles (neutral plus charged; 3 nm to 5 μm), and charged fraction of particles in the 2.5–25 nm diameter range. We developed qualitative and quantitative analysis tools to examine these data for contributions of IIN to new particle formation.

[44] We first report a simple theoretical analysis that identifies conditions under which measured charged fractions of particles in specified ranges can provide information about the initial charge state of the nucleated particles. Theory shows that freshly nucleated particles should "remember" the initial charge states for the range of growth rates observed in this study. The measured charged fractions during most of the events are below the stationary state values, and this discrepancy grew as size decreases; therefore neutral nucleation is the dominant process. By observing whether electrical charging or recombination dominates the particle current of intermediate ions, a qualitative conclusion can be made regarding whether the observed nanoparticle production is partially attributed to IIN. These analyses showed that positive and negative IIN contributed to nucleation on some days, while negative IIN was more important than positive IIN in a few cases, but do not provide quantitative information on the contributions of IIN to new particle formation.

[45] Next, quantitative analysis was performed to estimate the fractional contribution of positive and negative IIN to new particle formation rates for selected new particle formation events observed during this study. These analyses show that IIN contributed on average, only 0.5% of the particle current at 1 nm for both polarities. We conclude therefore that IIN contributed little to new particle formation during this study. The result is consistent with the direct mass spectrometric measurements of ion clusters performed at the same measurement site; the growth of $HSO_4^- \cdot (H_2SO_4)_x \cdot (H_2O)_y$, for values of x greater than 2 was not observed during nucleation events. Our conclusion is also consistent with the results predicated by recent numerical

ble 2. Measured Meteorological, Ion, and Aerosol Parameters During the High-Concentration Period in the Overlapping Size Range

MMDDYY[a]	T, °C	RH, %	SO_2,[b] ppb	Solar Radiation,[b] W m^{-2}	Ion Concentration, cm^{-3}		Z, cm^2 V^{-1} s^{-1}		Fuchs Surface Area, μm^2 cm^{-3}	Ion Production Rate, cm^{-3} s^{-1}	$dD_P/dt\|_\infty$, nm h^{-1}	$\Delta N/\Delta \log D_P$ (3.5–6 nm),[c] cm^{-3}	Measured Charged Fraction in 3.5–6 nm Range[d]		J_{1nm},[e] cm^{-3}–s	Fractional Contribution of IIN,[e] %	
					Positive	Negative	Positive	Negative					Positive, %	Negative, %		Positive, %	Negative, %
03/14/04	0.90	55.0	NA	399	964	735	1.40	1.74	40	5.2	4.5	1.0E+04	1.9	1.7	19	2.3	3.5
05/07/04	25.5	17.9	NA	921	604	414	1.53	2.08	65	4.5	6.1	1.0E+04	1.4	1.1	33	0.8	0.5
05/08/04	25.5	13.5	NA	697	1522	1303	1.54	1.87	30	3.1	6.7	5.0E+03	2.9	2.2	13	3.8	2.4
06/01/04	12.1	39.2	3.1	407	987	823	1.55	1.76	19	9.5	4.6	1.8E+04	1.5	1.4	37	0.4	0.4
06/02/04	16.1	44.3	0.58	855	634	455	1.54	1.98	64	6.7	3.5	2.4E+03	1.5	1.2	7.8	0.4	0.4
08/08/04	19.6	54.4	0.92	NA	952	883	1.57	1.87	63	6.6	5.7	5.2E+03	1.8	2.5	20	1.4	2.6
08/12/04	18.9	33.9	0.61	NA	660	470	1.47	1.89	61	7.6	5.2	7.4E+03	1.2	1.3	25	0.4	0.8
08/14/04	22.5	42.2	0.74	NA	736	672	1.44	1.86	106	8.1	3.0	7.0E+03	1.5	1.5	123	0.7	0.2
08/16/04	23.9	33.6	0.70	NA	662	624	1.51	2.02	82	9.1	4.3	3.3E+03	1.6	1.9	20	1.2	0.8
08/29/04	22.3	26.9	2.0	789	717	562	1.51	1.99	86	6.9	3.8	4.7E+03	1.4	1.3	21	0.4	0.1
09/03/04	20.0	38.9	NA	562	898	746	1.57	1.99	97	8.7	4.3	3.0E+03	2.1	1.9	15	1.4	1.3
09/06/04	17.5	39.5	2.1	568	720	656	1.56	1.88	71	6.6	3.1	7.4E+03	1.1	1.4	30	0.0	0.4
09/15/04	14.5	29.3	2.0	646	859	736	1.50	1.90	59	5.5	3.0	1.2E+04	1.3	1.4	118	0.0	0.0
09/20/04	21.8	41.6	1.0	694	690	593	1.58	2.01	120	5.2	5.2	6.6E+03	0.72	0.74	33	0.1	0.0
05/10/05	19.4	34.6	NA	833	607	418	1.57	2.04	195	5.2	7.6	1.1E+04	0.62	0.56	68	0.0	0.0
05/15/05	12.6	63.0	NA	623	725	559	1.54	1.77	111	6.3	3.7	6.1E+03	1.2	1.1	50	0.0	0.2
05/19/05	25.9	25.1	NA	NA	645	438	1.49	1.98	109	6.1	4.1	7.2E+03	0.88	0.81	26	0.0	0.0
05/21/05	25.8	24.5	NA	554	1103	818	1.47	1.90	85	4.1	5.3	2.0E+03	1.2%	1.2	10	0.0	0.1
05/22/05	19.7	55.4	NA	848	797	639	1.51	1.84	134	11	4.7	9.1E+03	1.0	0.87	42	0.1	0.0

[a]MMDDYY, month, day, and year.
[b]NA, not available.
[c]Read, for example, 1.0E + 04 as 1.0×10^4.
[d]Calculated using the 50th percentile value of the distribution of the SMPS concentration correction factor.
[e]Calculated by the simulation tool.

Table 3. Average Percent Contribution of the IIN of the Selected 19 Nucleation Events From March 2004 to May 2005 Defined in Terms of the Particle Production Rate (J) at 1 nm

Percentile Value of the Distribution of the SMPS Correction Factor, κ	Positive, %	Negative, %
50	0.42 (σ_g = 2.6)	0.40 (σ_g = 2.8)
84	1.0 (σ_g = 3.1)	1.1 (σ_g = 3.3)

models of ion-induced nucleation. It is possible that IIN may be more important in other regions of the atmosphere.

Notation

Symbols are listed in the order of appearance.

$f^{(\pm 1)}$ charged fraction of positive or negative particles.
N particle number concentration.
κ experimentally determined concentration correction factor for particles measured by the SMPS system in the overlapping size range.
n particle number distribution (number volume^{-1} size^{-1}).
$c^{\pm}$ concentrations of positive and negative small ions.
$D_P|_i$ particle size at size node i of numerical grid.
$D_P|_j$ representative particle size at size bin j of SMPS data.
$\beta_i^{(\pm,q)}$ ion-aerosol attachment coefficients between ±ions and particles with charge state q and size $D_P|_i$.
dD_P/dt diameter growth rate.
m_{vap} molecular mass of vapor.
ρ_{vap} density of a vapor molecule.
v_{vap} mean thermal speed of vapor.
c_{vap} concentration of vapor.
RM_i collision enhancement factor between condensing vapor and growing particle at size $D_P|_i$ due to their relative motion.
d_{vap} diameter of a vapor molecule.
$\Omega_i^{(q)}$ condensation enhancement factor of particles with charge state q at $D_P|_i$.
$\Gamma_i^{(q)}$ condensation sink by the preexisting particles for particles with charge state q at $D_P|_i$ (time^{-1}).
$\beta_{i,j}$ coagulation coefficient between electrically neutral particles of size $D_P|_i$ and $D_P|_j$.
$\Delta N_j^{(q)}$ concentration of particles in the jth size bin of the SMPS data with charge state q.
$W_{i,j}^{(q,p)}$ coagulation enhancement factor due to electrostatic potential between particles with charge state q and size $D_P|_i$ and particles with charge state p and size $D_P|_j$.
$\Phi_{i,j}^{(q,p)}$ electrostatic potential between particles with charge state q and size $D_P|_i$ and particles with charge state p and size $D_P|_j$.
J particle current (number volume^{-1} time^{-1}).
$\eta^{(\pm 1)}$ fractional contribution of ion-induced nucleation.
A_{Fuchs} Fuchs aerosol surface area (area/volume)

$$A_{Fuchs} = \frac{4\pi}{3}\sum_j \left(D_P|_j\right)^2 \left(\frac{Kn_j + Kn_j^2}{1+1.71Kn_j + 1.33Kn_j^2}\right)\Delta N_j.$$

Kn_j Knudsen number $2\lambda/D_P|_j$.
λ gas mean free ath.
T gas temperature.
ρ particle density.

[46] **Acknowledgments.** This article was prepared partly with support from EPA's NCER STAR Research Program, agreement R82962001. Support was also provided by DOE grant DE-FG-02-05ER63997. We also wish to express our appreciation to Hannes Tammet of the University of Tartu, Estonia, who built our IGMA and generously assisted us with its operation and maintenance, and to Katharine Moore, who operated the IGMA during the early part of this study.

References

Adachi, M., K. Okuyama, and Y. Kousaka (1983), Electrical neutralization of charged aerosol particles by bipolar ions, *J. Chem. Eng. Jpn.*, *16*(3), 229–235.
Biswas, S., P. M. Fine, M. D. Geller, S. V. Hering, and C. Sioutas (2005), Performance evaluation of a recently developed water-based condensation particle counter, *Aerosol Sci. Technol.*, *39*, 419–427.
Bricard, J. (1966), Electric charge and radioactivity of naturally occurring aerosols, in *Aerosol Science*, chap. 4, pp. 87–109, Elsevier, New York.
Chalmers, J. A. (1967), *Atmospheric Electricity*, Elsevier, New York.
Chen, D.-R., and D. Y. H. Pui (1999), A high efficiency, high throughput unipolar aerosol charger for nanoparticles, *J. Nanoparticle Res.*, *1*(1), 115–126.
Chen, D.-R., D. Y. H. Pui, D. Hummes, H. Fissan, F. R. Quant, and G. J. Sem (1998), Design and evaluation of a nanometer aerosol differential mobility analyzer (Nano-DMA), *J. Aerosol Sci.*, *29*(5/6), 497–509.
Eichkorn, S., S. Wilhelm, H. Aufmhoff, K. H. Wohlfrom, and F. Arnold (2002), Cosmic ray-induced aerosol-formation: First observational evidence from aircraft-based ion mass spectrometer measurements in the upper troposphere, *Geophys. Res. Lett.*, *29*(14), 1698, doi:10.1029/2002GL015044.
Eisele, F. L., E. R. Lovejoy, E. Kosciuch, K. F. Moore, R. L. Mauldin III, J. N. Smith, P. H. McMurry, and K. Iida (2006), Negative atmospheric ions and their potential role in ion-induced nucleation, *J. Geophys. Res.*, *111*, D04305, doi:10.1029/2005JD006568.
Fews, A. P., N. K. Holden, P. A. Keitch, and D. L. Henshaw (2005), A novel high-resolution small ion spectrometer to study ion nucleation of aerosols in ambient indoor and outdoor air, *Atmos. Res.*, *76*, 29–48.
Friedlander, S. K. (2000), *Smoke, Dust, and Haze: Fundamentals of Aerosol Dynamics*, Oxford Univ. Press, New York.
Fuchs, N. A. (1963), On the stationary charge distribution on aerosol particles in a bipolar ionic atmosphere, *Geofis. Pura Appl.*, *56*, 185–193.
Fuchs, N. A. (1964), *The Mechanics of Aerosols*, Macmillan, New York.
Gunn, R. (1954), Diffusion charging of atmospheric droplets by ions, and the resulting combination coefficients, *J. Meteorol.*, *11*(5), 339–347.
Hanson, D. R., and F. L. Eisele (2002), Measurement of prenucleation molecular clusters in the NH_3, H_2SO_4, H_2O system, *J. Geophys. Res.*, *107*(D12), 4158, doi:10.1029/2001JD001100.
Hering, S., M. Stolzenburg, F. Quant, D. Oberreit, and P. Keady (2005), A laminar-flow, water-based condensation particle counter (WCPC), *Aerosol Sci. Technol.*, *39*, 659–672.
Hinds, W. C. (1999), *Aerosol Technology: Properties, Behavior, and Measurement of Airborne Particles*, John Wiley, Hoboken, N. J.
Hoppel, W. A., and G. M. Frick (1986), Ion-aerosol attachment coefficients and the steady-state charge distribution on aerosols in bipolar ion environment, *Aerosol Sci. Technol.*, *5*, 1–21.
Hõrrak, U., J. Salm, and H. Tammet (1998a), Bursts of intermediate ions in atmospheric air, *J. Geophys. Res.*, *103*(D12), 13,909–13,915.
Hõrrak, U. M., A. Mirme, E. Tamm, and H. Tammet (1998b), Air ion measurements as a source of information about atmospheric aerosols, *Atmos. Res.*, *46*, 233–242.
Karlsson, M. N. A., and B. G. Martinsson (2003), Methods to measure and predict the transfer function size dependence of individual DMAs, *J. Aerosol Sci.*, *34*(50), 603–625.
Kim, T. O., M. Adachi, K. Okuyama, and J. H. Seinfeld (1997), Experimental measurement of competitive ion-induced and binary homogeneous nucleation in $SO_2/H_2O/N_2$ mixtures, *Aerosol Sci. Technol.*, *26*, 527–543.
Kulmala, M., H. Vehkamaki, T. Petaja, M. Dal Maso, A. Lauri, V.-M. Kerminen, W. Birmili, and P. H. McMurry (2004), Formation and growth rates of ultrafine atmospheric particles: A review of observations, *J. Aerosol Sci.*, *35*(2), 143–176.
Laakso, L., J. M. Mäkelä, L. Pirjola, and M. Kulmala (2002), Model studies on ion-induced nucleation in the atmosphere, *J. Geophys. Res.*, *107*(D20), 4427, doi:10.1029/2002JD002140.
Laakso, L., T. Anttila, K. E. J. Lehtinen, P. P. Aalto, M. Kulmala, U. Horrak, J. Paatero, M. Hanke, and F. Arnold (2004), Kinetic nucleation and

ions in boreal forest particle formation events, *Atmos. Chem. Phys.*, *4*(9/10), 2353–2366.
Lee, S.-H., J. M. Reeves, J. C. Wilson, D. E. Hunton, A. A. Viggiano, T. M. Miller, J. O. Ballenthin, and L. R. Lait (2003), Particle formation by ion nucleation in the upper troposphere and lower stratosphere, *Science*, *301*(5641), 1886–1889.
Liu, B. Y. H., and D. Y. H. Pui (1974), Equilibrium bipolar charge distribution of aerosols, *J. Colloid Interface Sci.*, *49*(2), 305–312.
Lovejoy, E. R., J. Curtius, and K. D. Froyd (2004), Atmospheric ion-induced nucleation of sulfuric acid and water, *J. Geophys. Res.*, *109*, D08204, doi:10.1029/2003JD004460.
McMurry, P. H., K. S. Woo, R. Weber, D.-R. Chen, and D. Y. H. Pui (2000), Size distributions of 3–10 nm atmospheric particles: Implications for nucleation mechanisms, *Philos. Trans. R. Soc. London, Ser. A*, *358*(1775), 2625–2642.
McMurry, P. H., et al. (2005), A criterion for new particle formation in the sulfur-rich Atlanta atmosphere, *J. Geophys. Res.*, *110*, D22S02, doi:10.1029/2005JD005901.
Nadykto, A. B., and F. Yu (2003), Uptake of neutral polar vapor molecules by charged clusters/particles: Enhancement due to dipole-charge interaction, *J. Geophys. Res.*, *108*(D23), 4717, doi:10.1029/2003JD003664.
Okuyama, K., M. Shimada, A. Okita, Y. Otani, and S. J. Cho (1998), Performance evaluation of cluster-DMA with integrated electrometer and its application to ion mobility measurements, *Earozoru Kenkyu*, *13*(2), 83–93.
Rader, D. J., and P. H. McMurry (1986), Application of the tandem differential mobility analyzer to studies of droplet growth or evaporation, *J. Aerosol Sci.*, *17*(5), 771–787.
Reischl, G. P., J. M. Mäkelä, R. Karch, and J. Necid (1996), Bipolar charging of ultrafine particles in the size range below 10 nm, *J. Aerosol Sci.*, *27*(6), 931–949.
Reiter, R. (1992), *Phenomena in Atmospheric and Environmental Electricity*, Elsevier, New York.
Seinfeld, J. H., and S. N. Pandis (1998), *Atmospheric Chemistry and Physics: From Air Pollution to Climate Change*, John Wiley, Hoboken, N. J.
Stolzenburg, M. R. (1988), An ultrainfe aerosol size distribution measuring system, Ph.D. thesis, Dep. of Mech. Eng., Univ. Minn., Minneapolis.
Stolzenburg, M. R., and P. H. McMurry (1991), An ultrafine aerosol condensation nucleus counter, *Aerosol Sci. Technol.*, *14*, 48–65.
Stolzenburg, M. R., P. H. McMurry, H. Sakurai, J. N. Smith, R. L. Mauldin III, F. L. Eisele, and C. F. Clement (2005), Growth rates of freshly nucleated atmospheric particles in Atlanta, *J. Geophys. Res.*, *110*, D22S05, doi:10.1029/2005JD005935.
Stolzenburg, M. R., K. Iida, P. H. McMurry, J. N. Smith and P. B. Keady (2006), Field evaluation of a water-based ultra-fine condensation particle counter, paper presented at 7th International Aerosol Conference, Am. Assoc. for Aerosol Res., St. Paul, Minn.
Tamm, E., U. Hõrrak, A. Mirme, and M. Vana (2001), On the charge distribution on atmospheric nanoparticles, paper presented at European Aerosol Conference, Eur. Aerosol Assem., Leipzig, Germany.
Tammet, H. (1995), Size and mobility of nanometer particles, clusters and ions, *J. Aerosol Sci.*, *26*(3), 459–475.
Tammet, H. (2002), Inclined grid mobility analyzer: The plain model, paper presented at Sixth International Aerosol Conference, Int. Aerosol Res. Assem., Taipei, Taiwan.
Tammet, H. (2003), Method of inclined velocities in the air ion mobility analysis, paper presented at 12th International Conference on Atmospheric Electricity 1, Int. Comm. on Atmos. Electr. of the Int. Assem. of Meteorol. and Atmos. Sci. of the Int. Union of Geod. and Geophys., Versailles, France.
Tammet, H., and M. Kulmala (2005), Simulation tool for atmospheric aerosol nucleation bursts, *J. Aerosol Sci.*, *36*(2), 173–196.
Tammet, H., J. Salm, and H. Iher (1988), Observation of condensation on small air ions in the atmosphere, *Lect. Notes Phys.*, *309*, 239–240.
Tammet, H., H. Iher, and J. Salm (1992), Spectrum of atmospheric ions in the mobility range of 0.32–3.2 cm2/(V·s), *Acta Comm. Univ. Tartu*, *947*, 35–49.
Vana, M., M. Kulmala, M. Dal Maso, U. Hõrrak, and E. Tamm (2004), Comparative study of nucleation mode aerosol particles and intermediate air ions formation events at three sites, *J. Geophys. Res.*, *109*, D17201, doi:10.1029/2003JD004413.
Wang, S. C., and R. C. Flagan (1990), Scanning electrical mobility spectrometer, *Aerosol Sci. Technol.*, *13*, 230–240.
Wiedensohler, A. (1988), An approximation of the bipolar charge distribution for particles in the submicron size range, *J. Aerosol Sci.*, *19*(3), 387–389.
Wiedensohler, A., E. Luetkemeier, M. Feldpausch, and C. Helsper (1986), Investigation of the bipolar charge distribution at various gas conditions, *J. Aerosol Sci.*, *17*(3), 413–416.
Wilhelm, S., S. Eichkorn, D. Wiedner, L. Pirjola, and F. Arnold (2004), Ion-induced aerosol formation: New insights from laboratory measurements of mixed cluster ions $HSO_4^-(H_2SO_4)_a(H_2O)_w$ and $H + (H_2SO_4)_a(H_2O)_w$, *Atmos. Environ.*, *38*(12), 1735–1744.
Yu, F. (2006), From molecular clusters to nanoparticles: Second-generation ion-mediated nucleation model, *Atmos. Chem. Phys. Discuss.*, *6*, 3049–3092.
Yu, F., and R. P. Turco (2000), Ultrafine aerosol formation via ion-mediated nucleation, *Geophys. Res. Lett.*, *27*(6), 883–886.
Yu, F., and R. P. Turco (2001), From molecular clusters to nanoparticles: Role of ambient ionization in tropospheric aerosol formation, *J. Geophys. Res.*, *106*(D5), 4797–4814.
Yue, G., and L. Chan (1979), Theory of formation of volatile binary solutions through the ion-induced nucleation process, *J. Colloid Interface Sci.*, *68*(3), 501–507.
Zhang, S.-H., and R. C. Flagan (1996), Resolution of the radial differential mobility analyzer for ultrafine particles, *J. Aerosol Sci.*, *27*(8), 1179–1200.
Zhang, S.-H., Y. Akutsu, L. M. Russell, R. C. Flagan, and J. H. Seinfeld (1995), Radial differential mobility analyzer, *Aerosol Sci. Technol.*, *23*, 357–372.

M. J. Dunn, F. Eisele, and J. N. Smith, Atmospheric Chemistry Division, National Center for Atmospheric Research, 1850 Table Mesa Drive, Boulder, CO 80305, USA.

K. Iida, P. McMurry, and M. Stolzenburg, Particle Technology Laboratory, University of Minnesota, 111 Church Street, SE, Minneapolis, MN 55455, USA. (iida@me.umn.edu)

P. Keady, Quant Technologies, LLC, 1463 94th Lane NE, Blaine, MN 55449, USA.